Received: 4 October 2017 | Revised: 3 April 2018 | Accepted: 6 April 2018 | Uncorrected manuscript published: 14 April 2018 | Published on: 17 May 201
DOI: 10.1111/tra.12572

WILEY Traffic

ORIGINAL ARTICLE

The kinases male germ cell-associated kinase and cell cycle-related kinase regulate kinesin-2 motility in *Caenorhabditis elegans* neuronal cilia

Peishan Yi | **Chao Xie** | **Guangshuo Ou**

Tsinghua-Peking Center for Life Sciences, School of Life Sciences and MOE Key Laboratory for Protein Science, Tsinghua University, Beijing, China

Correspondence
Guangshuo Ou, Tsinghua-Peking Center for Life Sciences, School of Life Sciences and MOE Key Laboratory for Protein Science, Tsinghua University, Beijing 100084, China.
Email: guangshuoou@tsinghua.edu.cn

Funding information
National Basic Research Program of China, Grant/Award Number: 2017YFA0503501; National Natural Science Foundation of China, Grant/Award Number: 31525015; 31561130153; Newton Advanced Fellowship, Grant/Award Number: 140490.

Kinesin-2 motors power anterograde intraflagellar transport (IFT), a highly ordered process that assembles and maintains cilia. However, it remains elusive how kinesin-2 motors are regulated in vivo. Here, we performed forward genetic screens to isolate suppressors that rescue the ciliary defects of OSM-3-kinesin (homolog of mammalian homodimeric kinesin-2 KIF17) mutants in *Caenorhabditis elegans*. We identified the *C. elegans dyf-5* and *dyf-18*, which encode the homologs of mammalian male germ cell-associated kinase and cell cycle-related kinase, respectively. Using time-lapse fluorescence microscopy, we show that DYF-5 and DYF-18 are IFT cargo molecules and are enriched at the distal segments of sensory cilia. Mutations of *dyf-5* and *dyf-18* generate elongated cilia and ectopic localization of the heterotrimeric kinesin-2 (kinesin-II) at the ciliary distal segments. Genetic analyses reveal that *dyf-5* and *dyf-18* are important for stabilizing the interaction between IFT particles and OSM-3-kinesin. Our data suggest that DYF-5 and DYF-18 act in the same pathway to promote handover between kinesin-II and OSM-3 in sensory cilia.

KEYWORDS
CCRK, cilia, intraflagellar transport, kinesin-2, MAK

1 | INTRODUCTION

Cilia are microtubule-based organelles that play important roles in signal sensation and motility.[1] The assembly and maintenance of cilia rely on intraflagellar transport (IFT), a process first discovered in *Chlamydomonas* and later found in various ciliated organisms.[2–6] This process exploits multiprotein complexes—IFT particles—to transport various ciliary components bidirectionally between the ciliary base and tip.[4,5] Anterograde IFT, namely, the transport of IFT components from the ciliary base to the tip, is driven by the kinesin-2 motors, whereas the retrograde transport of IFT components from the tip to the base is powered by the cytoplasmic dynein-2.

Abbreviations: CCRK, cell cycle-related kinase; Dyf, dye-filling defective; EMS, ethyl methanesulfonate; IFT, intraflagellar transport; KAP, kinesin-associated subunit; MAK, male germ cell-associated kinase; RCK, *ros-cross* hybridizing kinase; WT, wild type

The nematode *Caenorhabditis elegans* is a valuable model organism for identifying and investigating IFT components including kinesin-2 motors. The heterotrimeric kinesin-2 (kinesin-II), which is composed of 2 different motor subunits and a kinesin-associated subunit (KAP), is employed by most species to power the anterograde IFT.[7] The assembly of *C. elegans* sensory cilia requires another homodimeric kinesin-2 OSM-3.[7–10] In *C. elegans* amphid and phasmid sensilla, cilia are assembled into bipartite structures that contain a middle segment with 9 doublet microtubules and a distal segment with 9 singlet microtubules.[11] Kinesin-II is restricted to the middle segments, while OSM-3 moves along the entire cilium.[8,12,13] Genetic studies demonstrate that OSM-3 and kinesin-II co-operate to build the middle segments whereas OSM-3 alone assembles the distal segments of sensory cilia.[8,12] The handover mechanism between kinesin-II and OSM-3 in anterograde transport has been recently demonstrated: kinesin-II is required for efficient import of IFT particles from the cell body into the ciliary compartment, whereas OSM-3 mediates

long-distance transport along the entire cilium.[13] However, how they are controlled to move synergistically along the axoneme is not well understood.

The precise localization and regulation of kinesin motors are essential for coherent intracellular transport.[7,14] The activity of kinesin-2 motors can be modulated through an autoinhibitory mechanism. For instance, OSM-3 and its mammalian homolog KIF17 are autoinhibited by residing in a compact conformation with the involvement of interactions between the tail and motor domains.[15,16] Perturbation of these interactions or mimicking cargo loading, which is believed to maintain the extended active conformation, produces enhanced motility and processivity. It is unclear how the autoinhibitory mechanism applies to the regulation of OSM-3 activity during ciliogenesis. A simple model is that OSM-3 becomes active once it is docked onto IFT particles, and this model is supported by the observation that loss of the IFT component DYF-1/IFT70 inactivates OSM-3 motility.[12] However, no direct interaction between DYF-1 and OSM-3 has been reported, and DYF-1 alone fails to activate OSM-3 in vitro.[16] Additional evidence comes from the analyses of the *sa125* mutation of OSM-3, which converts a glycine to glutamate (G444E) in the hinge region and relieves the autoinhibited state without cargo binding in single-molecule assays.[16] Interestingly, the *osm-3(sa125)* mutant forms defective cilia, similar to an *osm-3* null mutant.[8] It is thought that OSM-3(G444E) may become constitutively active and fail to bind IFT cargos, making it unable to be assembled or travel into cilia.[16]

The autoinhibitory mechanism of the classical heterotrimeric kinesin-II is less completely understood, although its folded and extended conformations have been observed under electron microscopy.[17] An in vitro study shows that mutations in the coiled coil region increase the motility and processivity of heterodimerized motor subunits of kinesin-II.[18] Phosphorylation can provide another layer of regulation of kinesin-II activity and localization in cilia. The *Chlamydomonas* kinesin-II motor subunit FLA8/KIF3B is phosphorylated and inactivated by the calcium-dependent kinase CDPK1, which inhibits IFT entry probably by disrupting the interactions between kinesin-II and IFT particles.[19] Other kinases, including cell cycle-related kinase (CCRK), *ros-cross* hybridizing kinase (RCK) family members (MAK, ICK and MOK) and their homologs in *Chlamydomonas*, *C. elegans* and other species, have been implicated in the inhibition of kinesin-II due to the long-cilia phenotypes in their absence.[20–30] MAK and ICK are substrates of CCRK.[23,31,32] ICK is reported to phosphorylate the mammalian kinesin-II motor subunit KIF3A.[21] However, CCRK and its homologs do not localize to cilia, which is inconsistent with the site of their action.[23,25,33,34] MAK/ICK and their homologs are reported to localize to the entire cilium,[22] the ciliary base[20,26] or the ciliary tip.[21,23,24] The localization of ICK can be either dependent[20] or independent of its kinase activity.[21,22]

Here we report that the OSM-3 hinge mutation G444E is insufficient to constitutively activate it in vivo. In contrast, OSM-3(G444E) motility is compromised. In our attempt to isolate suppressors of *osm-3(G444E)*, we have identified 2 kinases, DYF-5/MAK and DYF-18/CCRK. DYF-5 and DYF-18 are IFT cargo molecules required for restricting the kinesin-II to the middle segments. Genetic analyses suggest that DYF-5 and DYF-18 act in the same pathway to regulate the co-ordination between kinesin-II and OSM-3. We propose a model in which DYF-5 and DYF-18 promote the handover between kinesin-II and OSM-3. Defects in this process lead to ectopic kinesin-II localization and reduced recycling efficiency.

2 | RESULTS

2.1 | OSM-3 motility is severely compromised by the hinge mutation G444E in vivo

The autoinhibition model infers that the G444E mutation in the hinge region (H2) relieves autoinhibition of OSM-3 without cargo loading[16] (Figure 1A). To test this possibility in vivo, we overexpressed Green Fluorescent Protein (GFP)-labeled OSM-3(G444E) under the control of a ciliated neuron-specific promoter (P*dyf-1*) in wild type (WT) *C. elegans*. Surprisingly, we found that both amphid and phasmid sensory cilia were severely truncated in the transgenic animals, phenocopying the G444E mutant *osm-3(sa125)* or the null mutant *osm-3 (p802)* (Figure 1B-D). Overexpression of OSM-3 with a small deletion in the hinge region (ΔH2) resulted in the same phenotypes (Figure 1E). In the remaining middle segments, OSM-3(G444E) moved at 0.63 ±0.16 μm/s (mean ±SD, *N* = 184) in the anterograde direction, which is slower than the WT velocity (0.7-0.8 μm/s at the middle segments, Table 1).[8] The mCherry-labeled IFT particle-B subcomplex component OSM-6/IFT52 traveled at a similar speed (0.65. ±0.10 μm/s, mean ±SD, *N* = 123). These results suggest that OSM-3 (G444E) is not constitutively active. Instead, its motility is compromised, and OSM-3(G444E) interferes with the function of the endogenous OSM-3.

To further test this possibility, we expressed OSM-3(G444E)::GFP under the control of a heat-shock-inducible promoter (P*hsp-16.2*). Low-level expression was induced at room temperature without heat shock, which did not affect cilium assembly, allowing the measurement of velocity in the intact cilia (Figure 1F). In the middle and distal segments, OSM-3(G444E) moved at 0.68 ±0.15 μm/s (mean ±SD, *N* = 144) and 1.03 ±0.17 μm/s (mean ±SD, *N* = 116), respectively, which are slower than the WT velocities (Table 1). Robust expression induced by heat-shock treatment caused severe truncation of the distal segments, similar to that caused by expressing OSM-3(G444E):: GFP under the control of P*dyf-1* (Figure 1E,G). Furthermore, OSM-3 (G444E)::GFP formed aggregates at the ciliary base and tip (Figure 1G). These results further support a model in which OSM-3 (G444E) is not fully active. Because multiple motor proteins can be engaged in association with the same cargo, OSM-3(G444E) can be inactive but moves as part of the cargo transported by endogenous motors. However, it is also possible that OSM-3(G444E) is active but with reduced motility and synergistically transports cargos with kinesin-II and endogenous OSM-3.

To exclude the effects of endogenous OSM-3, we expressed OSM-3(G444E)::GFP and an mCherry-labeled version of the kinesin-II subunit KAP-1 in the G444E mutant *osm-3(sa125)*. OSM-3(G444E) and KAP-1 moved at 0.56 ±0.12 μm/s (mean ±SD, *N* = 138) and 0.57 ±0.11 μm/s (mean ±SD, *N* = 62), respectively. To distinguish whether OSM-3(G444E) is passively transported by kinesin-II or moves at a similar speed, we examined OSM-3(G444E) motility in the

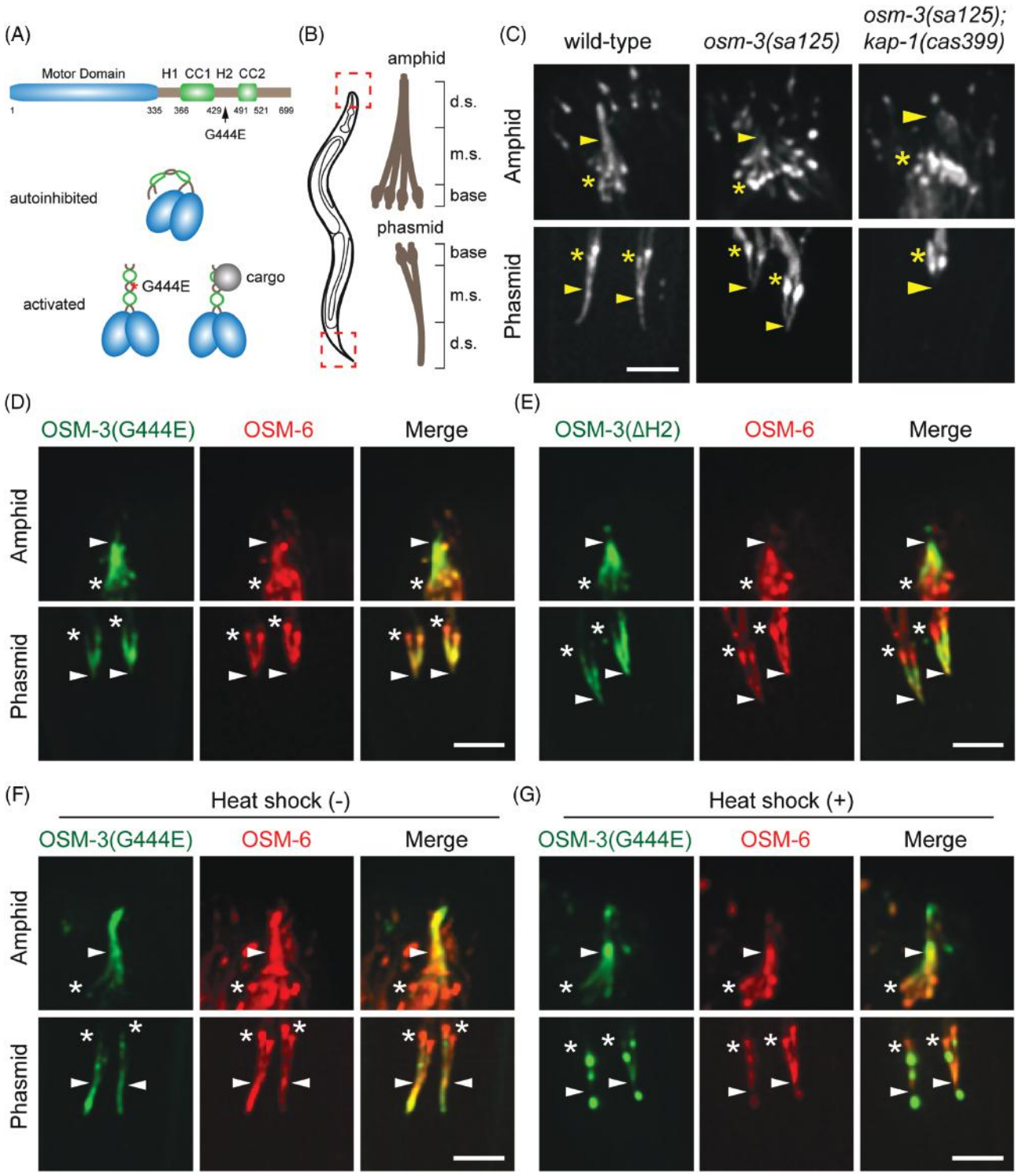

FIGURE 1 OSM-3(G444E) impairs cilium formation. (A) Domain structures of OSM-3 and the autoinhibition model. The motor domain (blue), coiled-coil domains (CC1 and CC2) and hinge regions (H1 and H2) are indicated. In the autoinhibited state, the OSM-3 tail folds back to generate a compact conformation. Cargo loading or the G444E mutation in hinge 2 relieves autoinhibition. (B) Schematic depiction of the *Caenorhabditis elegans* amphid and phasmid cilia. Ten or 2 sensory cilia are aligned into the amphid or phasmid channels (dashed boxes and enlarged on the right), respectively. Each cilium contains a ciliary base, a middle segment (m.s.) and a distal segment (d.s.). The distal segments are exposed to the environment (not shown). (C) Amphid (top) and phasmid (bottom) cilia in the WT, G444E mutant *osm-3(sa125)* and *osm-3; kap-1* double-mutant animals. Cilia are marked with GFP-tagged IFT52/OSM-6. Star, ciliary base; arrowhead, junction between the middle and distal segments; scale bar, 5 μm (the same as in [D-G]). (D) Ciliary phenotypes in OSM-3(G444E) transgenic animals. OSM-3(G444E)::GFP and OSM-6::mCherry are expressed under the control of P*dyf-1*, a ciliated neuron-specific promoter. (E) Ciliary phenotypes in OSM-3(ΔH2) transgenic animals. OSM-3 (ΔH2)::GFP and OSM-6::mCherry are expressed under the control of P*dyf-1*. ΔH2, deletion of hinge 2. (F) Ciliary phenotypes in OSM-3(G444E) transgenic animals. OSM-3(G444E)::GFP is expressed under the control of the heat shock promoter P*hsp-16.2* without heat shock treatment. OSM-6::mCherry is expressed under the control of the P*dyf-1* promoter. (G) Ciliary phenotypes in OSM-3(G444E) transgenic animals. OSM-3 (G444E)::GFP is expressed under the control of P*hsp-16.2* after a 1-hour heat shock treatment at 33°C

TABLE 1 Summary of IFT velocities

Genotype	Anterograde (m.s.)	Anterograde (d.s.)	Retrograde
WT	0.76 ± 0.12 (302)	1.29 ± 0.24 (206)	1.24 ± 0.20 (88)
osm-3(p802)	0.58 ± 0.07 (332)	None	N/A
osm-3(sa125)	0.61 ± 0.08 (208)	None	N/A
dyf-5(cas357)	0.67 ± 0.21 (316)	0.82 ± 0.20 (208)	1.19 ± 0.28 (255)
dyf-18(cas390)	0.76 ± 0.21 (148)	0.95 ± 0.25 (128)	1.25 ± 0.31 (142)
dyf-18(ok200)	0.63 ± 0.10 (149)	0.67 ± 0.08 (74)	1.24 ± 0.20 (82)
osm-3(sa125); dyf-5(cas357)	0.65 ± 0.10 (322)	0.64 ± 0.14 (77)	1.20 ± 0.27 (99)
osm-3(sa125); dyf-18(cas390)	0.57 ± 0.09 (150)	0.58 ± 0.09 (66)	1.14 ± 0.18 (42)
osm-3(sa125); dyf-5(cas357); dyf-18(cas390)	0.59 ± 0.09 (183)	Undetectable	1.10 ± 0.24 (53)
kap-1(cas399)	1.24 ± 0.19 (174)	1.26 ± 0.30 (80)	N/A
kap-1(cas399); dyf-18(ok200)	0.92 ± 0.20 (130)	1.27 ± 0.36 (121)	N/A
kap-1(cas399); dyf-5(cas357)	1.28 ± 0.22 (181)	1.31 ± 0.22 (148)	N/A

Abbreviations: m.s., middle segment; d.s., distal segment; N/A, not available. Velocities are quantified using GFP-labeled IFT52/OSM-6 (mean ± SD, μm/s). The numbers of particles used for quantification are indicated in the brackets.

osm-3(sa125); bbs-8(nx77) double mutant. Notably, *bbs-8* is a BBSome component,[35] and its absence induces the separation of IFT particles into 2 halves: the IFT-A subcomplex transported by kinesin-II and the IFT-B subcomplex transported by OSM-3.[12] We found that the movement of OSM-3(G444E) was completely undetectable in 5 out of 10 movies in the *osm-3(sa125); bbs-8(nx77)* double mutant. In the remaining cases, OSM-3(G444E) occasionally moved at a speed of 0.58 ±0.06 μm/s (mean ±SD, N = 16). These results demonstrate that the G444E mutation severely compromises OSM-3 motility in vivo and that OSM-3(G444E) remains associated with IFT particles.

2.2 | Mutations of *dyf-5* and *dyf-18* suppress ciliary defects in *osm-3(sa125)*

As in vitro results suggest that G444E causes conformational changes in OSM-3,[16] we speculate that essential intermolecular or intramolecular interactions might be disrupted by G444E and that defects in IFT may be rescued by other mutations in OSM-3 or its regulators. To seek for such mutations, we performed suppressor screening of the G444E mutant *osm-3(sa125)* (Figure 2A). We identified 2 genes, *dyf-5* and *dyf-18*, whose mutations rescued the dye-filling defects (Dyf) of *osm-3(sa125)* (Figure 2B,C). *dyf-5* encodes the homolog of mammalian *rck* family members and *Chlamydomonas long-flagella 4* (*lf4*). *dyf-18* is homologous to mammalian *ccrk* and *Chlamydomonas long-flagella 2* (*lf2*). We obtained 3 alleles of *dyf-5* and 8 alleles of *dyf-18* (Figure 2B, C). All mutations introduce amino acid changes in the conserved kinase domains except 2 alleles of *dyf-18*, *cas387* and *cas392* (Figure S1A in Appendix S1, Supporting Information). *cas387* is a G-to-A conversion at the splicing site following exon 5, and *cas392* converts a conserved cytosine to thymine in the X-box motif residing in the 5′UTR. The X-box motif is essential for ciliary gene expression.[36]

We next examined the ciliary phenotypes in these suppressors. Using GFP-labeled OSM-6/IFT52, a component of the IFT-particle B subcomplex, we found that the distal segments of amphid and phasmid cilia were restored. Cilium length increased from 4.3 to ~7.3 μm (Figure 2D,F). Tubulin markers specific for ciliated neurons also indicate that axoneme assembly is partially rescued (Figure S2A-C in Appendix S1). We next introduced 2 other independent alleles, *ok200* (a deletion allele from *Caenorhabditis* Genetics Center) and *cas444* (a frame-shift allele constructed by CRISPR/Cas9 knockout), of *dyf-18* into the *osm-3 (sa125)* mutant. Cilium length was fully restored, similarly demonstrating that *dyf-18* is a true suppressor gene (Figure 2D,F). As overexpression of *dyf-5* causes the Dyf phenotype,[26] we cannot perform a rescue experiment to demonstrate that *dyf-5* is responsible for the suppression. However, the isolation of multiple independent alleles suggests that *dyf-5* is a suppressor gene. In addition, *dyf-5(cas357)* decreased the Dyf phenotype of the *osm-3(p802)* null mutant from 100% to 43% (N = 141). However, the *dyf-5* null mutation *mn400* did not suppress the Dyf phenotype of either *osm-3(sa125)* or *osm-3(p802)*.

Next, we examined the ciliary phenotypes in *dyf-5* or *dyf-18* single mutants. We found that the cilium length was markedly increased in *dyf-5* single mutant, which is consistent with a previous report.[26] Similar phenotypes have been observed when its homologs in *Chlamydomonas* and mammalian cells are mutated or knocked down[20,22,24,28,29] (Figure 2E,F). The *dyf-18* mutant also possesses longer cilia, although to a lesser extent (Figure 2E,F). This phenotype is consistent with the findings in *Chlamydomonas lf2* mutant flagella and cilia of mammalian cells in which *ccrk* is knocked down.[23,25,29,30] However, in the dye-filling assay, all *dyf-18* mutants showed a subtle Dyf phenotype. To further verify that the cilium length is properly measured using the GFP-tagged IFT markers, we performed intensity plot of multiple randomly selected mutant cilia. We showed that the ciliary bases can be faithfully characterized at a size of 0.6 μm (Figure S2D in Appendix S1). This value is comparable to the SD of cilium-length measurement in the WT cilia (0.7 μm), which indicates that the variation in the size of ciliary bases does not substantially affect cilium-length measurement. Moreover, the Dyf and cilium-length phenotypes of *dyf-5* and *dyf-18* are consistent with previous reports that cilium length is significantly increased in *dyf-5* mutant and that the absence of *dyf-18* causes occasional cilium elongation and mild Dyf phenotype.[26,34] Interestingly, in contrast to the *dyf-5* null mutant, which shows a complete Dyf phenotype, our isolated *dyf-5* mutants only showed mild Dyf phenotypes. We speculate that these mutations may cause weak loss of function. Indeed, IFT velocities were dramatically decreased, to ~0.5 μm/s, in the *dyf-5* null mutant,[26] but were partially reduced in our mutants. Moreover, the *dyf-5* null

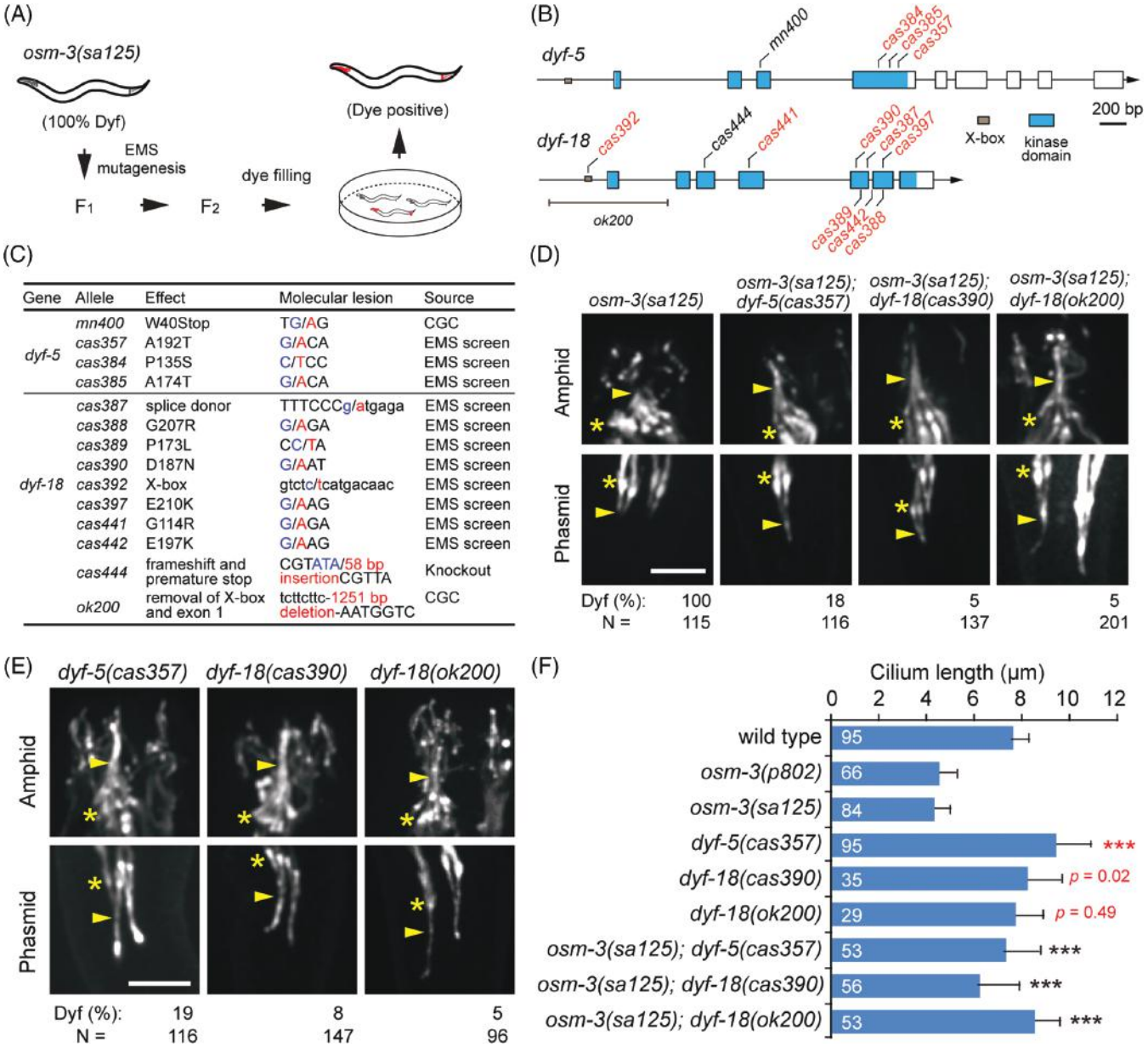

Gene	Allele	Effect	Molecular lesion	Source
dyf-5	*mn400*	W40Stop	TG/AG	CGC
	cas357	A192T	G/ACA	EMS screen
	cas384	P135S	C/TCC	EMS screen
	cas385	A174T	G/ACA	EMS screen
dyf-18	*cas387*	splice donor	TTTCCCg/atgaga	EMS screen
	cas388	G207R	G/AGA	EMS screen
	cas389	P173L	CC/TA	EMS screen
	cas390	D187N	G/AAT	EMS screen
	cas392	X-box	gtctc/tcatgacaac	EMS screen
	cas397	E210K	G/AAG	EMS screen
	cas441	G114R	G/AGA	EMS screen
	cas442	E197K	G/AAG	EMS screen
	cas444	frameshift and premature stop	CGTATA/58 bp insertionCGTTA	Knockout
	ok200	removal of X-box and exon 1	tcttcttc-1251 bp deletion-AATGGTC	CGC

FIGURE 2 Mutations of *dyf-5* and *dyf-18* suppress ciliary defects in the *osm-3(sa125)* mutant. (A) Flowchart of the suppressor screening. *osm-3 (sa125)* animals are 100% dye-filling defective (Dyf). Animals at the late L4 stage were treated with ethyl methanesulfonate (EMS). F2 progenies were screened by filling with the fluorescent dye DiI. Dye-positive animals were considered putative suppressors. The ciliary phenotypes were verified via microscopy. Mutant genes were cloned by single-nucleotide polymorphism mapping (see Section 4). (B) Genomic structures of *dyf-5* (isoform a) and *dyf-18*. Exons are marked with large boxes. Blue regions indicate the coding sequence of the kinase domain. Small boxes in gray are X-box motifs within the promoters. Alleles isolated by EMS screening are in red. Other alleles are in black. Scale bar, 200 bp. (C) Details of the *dyf-5* and *dyf-18* alleles. *cas444* was constructed by CRISPR/Cas9-triggered genome editing. CGC, *Caenorhabditis* Genetics Center. (D) Ciliary phenotypes in the *osm-3* single mutant and the *osm-3; dyf-5* and *osm-3; dyf-18* double mutants. Cilia are visualized with GFP-tagged IFT52/OSM-6. Dyf, dye-filling defective; star, ciliary base; arrowhead, junction between the middle and distal segments; scale bar, 5 μm (the same as in [E]). (E) Ciliary phenotypes in *dyf-5* and *dyf-18* single mutants. (F) Quantification of cilium length (mean ±SD.). Numbers of worms are indicated in the bars. Red stars or *P* values represent the comparisons between the WT and mutant animals; black stars represent the comparisons between the *osm-3(sa125)* single mutant and the double mutants. ***, $P < .001$, 2-tailed Student's *t* test

allele cannot suppress the Dyf of *osm-3(G444E)*. These data show that *dyf-5* and *dyf-18* are required for ciliogenesis, but the absence of *dyf-18* or the partial loss of function of *dyf-5* does not completely block IFT and ciliogenesis (Figure 2E). Consistently, only mild accumulation of IFT particles at the ciliary tip was observed, and IFT was detectable along the full length of cilia in their mutants, although the speed was slower than that in WT animals (Figure 2E, Table 1).

2.3 | DYF-5 and DYF-18 restrict kinesin-II to the middle segment

A previous study has shown that loss of *dyf-5* leads to the ectopic entry of kinesin-II into the distal segments.[26] We asked whether the suppression by *dyf-5* and *dyf-18* was a consequence of functional compensation by kinesin-II in the distal segments. Considering that the 3 alleles of *dyf-5* exhibit the same phenotypes and that *ok200* is

putatively null, we used *cas357* and *ok200* to investigate the roles of *dyf-5* and *dyf-18*, respectively, in ciliogenesis. Using the kinesin-II marker KAP-1::GFP, we found that kinesin-II ectopically entered the distal segments in both mutants (Figure 3A). A similar localization pattern was observed when a GFP-labeled version of the endogenous kinesin-II motor subunit KLP-20/KIF3A was examined (Figure 3B). To further test whether kinesin-II is required for suppression of *osm-3 (sa125)*, we generated the *dyf-5(cas357); kap-1(cas399)* and *osm-3 (sa125)* triple mutant. As expected, this mutant was 100% Dyf, and the distal segments cannot be restored, indicating that kinesin-II is required for suppression. Interestingly, compared with the *kap-1 (cas399); osm-3(sa125)* double mutant which lacks both middle and distal segments (Figure 1C), the triple mutant formed middle segments (Figure 3C). IFT was detectable at a speed of 0.53 ±0.09 μm/s (mean ±SD, *N* = 95), suggesting that, in the absence of kinesin-II, the loss of function of *dyf-5* promotes the capability of OSM-3(G444E) in driving IFT (Figure 3C). This result also supports that OSM-3(G444E) alone retains partial activity.

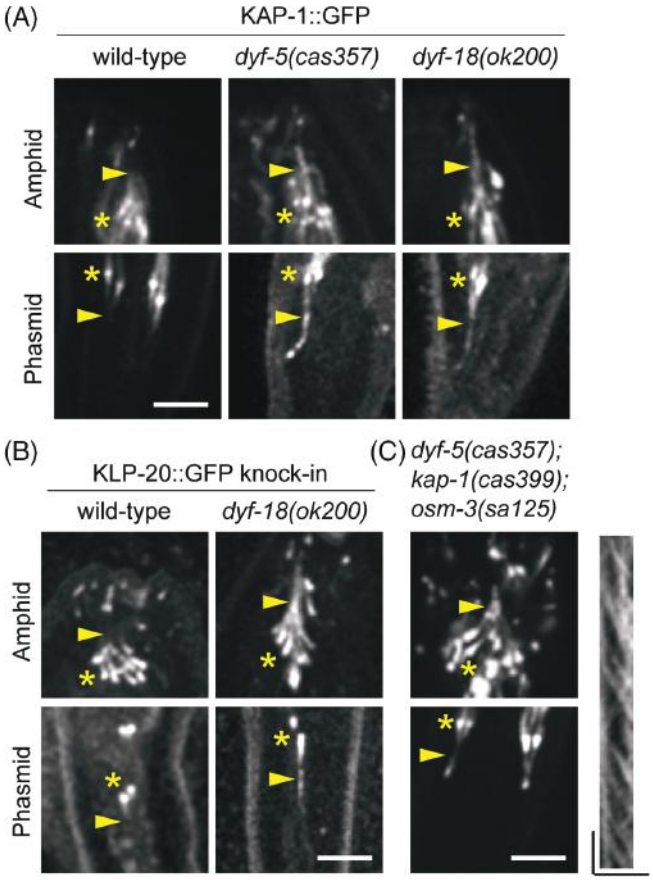

FIGURE 3 Kinesin-II enters the distal segments in *dyf-5* and *dyf-18* mutants. (A) Localization of GFP-labeled kinesin-II accessory subunit (KAP-1/KAP) in WT and mutant worms. Star, ciliary base; arrowhead, junction between the middle and distal segments; scale bar, 5 μm (the same as in [B]). (B) Localization of GFP-labeled endogenous kinesin-II motor subunit (KLP-20/KIF3A) in WT and *dyf-18* mutant worms. (C) Ciliary phenotypes in *dyf-5; kap-1* and *osm-3* triple-mutant animals. Cilia are marked with GFP-tagged IFT52/OSM-6. Kymograph shows IFT in the middle segments. Star, ciliary base; arrowhead, junction between the middle and distal segments; scale in image, 5 μm; scales in kymograph: horizontal, 5 μm; vertical, 5 seconds

2.4 | DYF-5 and DYF-18 fine-tune the co-ordination between kinesin-II and OSM-3

Next, we asked how DYF-5 and DYF-18 regulate OSM-3-kinesin. In *dyf-5* or *dyf-18* single mutants, IFT velocities at the middle and distal segments were both reduced, indicative of reduced OSM-3 motility (Table 1). In contrast, the retrograde IFT speed was normal (Table 1). To quantify the velocity of OSM-3-driven IFT alone, we generated the *dyf-5; kap-1* and *dyf-18; kap-1* double mutants. Unexpectedly, we found that IFT velocities were largely comparable to the IFT speed driven by OSM-3 alone (~1.3 μm/s) in the *kap-1* single mutant (Figure 4A-C, Table 1).[8] Speed in the middle segments of the *dyf-18; kap-1* double mutant became slower (Table 1). These data suggest that DYF-5 and DYF-18 may not affect OSM-3 activity but instead regulate the stability of OSM-3 and IFT-particle interactions. In support of this notion, we observed decreases in IFT frequency in *dyf-5; kap-1* and *dyf-18; kap-1* double mutants (Figure 4D). Therefore, in *dyf-5* and *dyf-18* single mutants, it is probably that IFT particles are predominantly transported by the slower kinesin-II; however, OSM-3 still weakly binds to IFT particles. As IFT frequency also deceases in *dyf-5* and *dyf-18* single mutants, we reasoned that the efficiencies of IFT driven by both kinesin-II and OSM-3 are reduced when the co-ordination between kinesin-II and OSM-3 becomes defective. Considering that kinesin-II enters distal segments in the absence of *dyf-5* or *dyf-18*, we propose that DYF-5 and DYF-18 function to promote the handover of IFT particles between kinesin-II and OSM-3. Loss of their function results in the failure of undocking kinesin-II and the docking of OSM-3, which is consistent with previous findings.[26]

2.5 | Mutations of *dyf-5* and *dyf-18* impair recycling of IFT components

The similar ciliary phenotypes in *dyf-5* and *dyf-18* mutants suggest that they may function in the same pathway. To test this, we generated the *osm-3(sa125); dyf-5(cas357)* and *dyf-18(cas390)* triple-mutant animal. This mutant was completely Dyf, and IFT particles were strongly accumulated at the distal segments (Figure 4E). However, the cilium length was comparable to that of *osm-3(sa125); dyf-5(cas357)* or *osm-3(sa125)* and *dyf-18(cas390)* double-mutant animals. Moreover, we observed ectopic localization of kinesin-II in *dyf-5; dyf-18* double mutant (Figure 4F). These data further support the notion that DYF-5 and DYF-18 act in the same pathway on cilium assembly and regulation of kinesin-II.

Next, we explored the accumulation of IFT particles at the distal segments of the *dyf-5(cas357); dyf-18(cas390)* double mutant. In contrast to the accumulation of IFT particles at the ciliary tips or occasionally at the junction between the middle and distal segments of each single mutant (Figure 2E), kinesin-II, OSM-3, cytoplasmic dynein-2 and IFT particles all formed sizeable aggregates throughout the distal segments (Figure 4F). Retrograde velocity was undetectable in the distal segments due to strong aggregation but was normal in the middle segments and in the cilia of *dyf-5* or *dyf-18* single mutants (Table 1). Taken together, these data indicate that *dyf-5* and *dyf-18* regulate efficient recycling of IFT components. Because reorganization of IFT particles is critical for retrograde transport initiation,[37] the

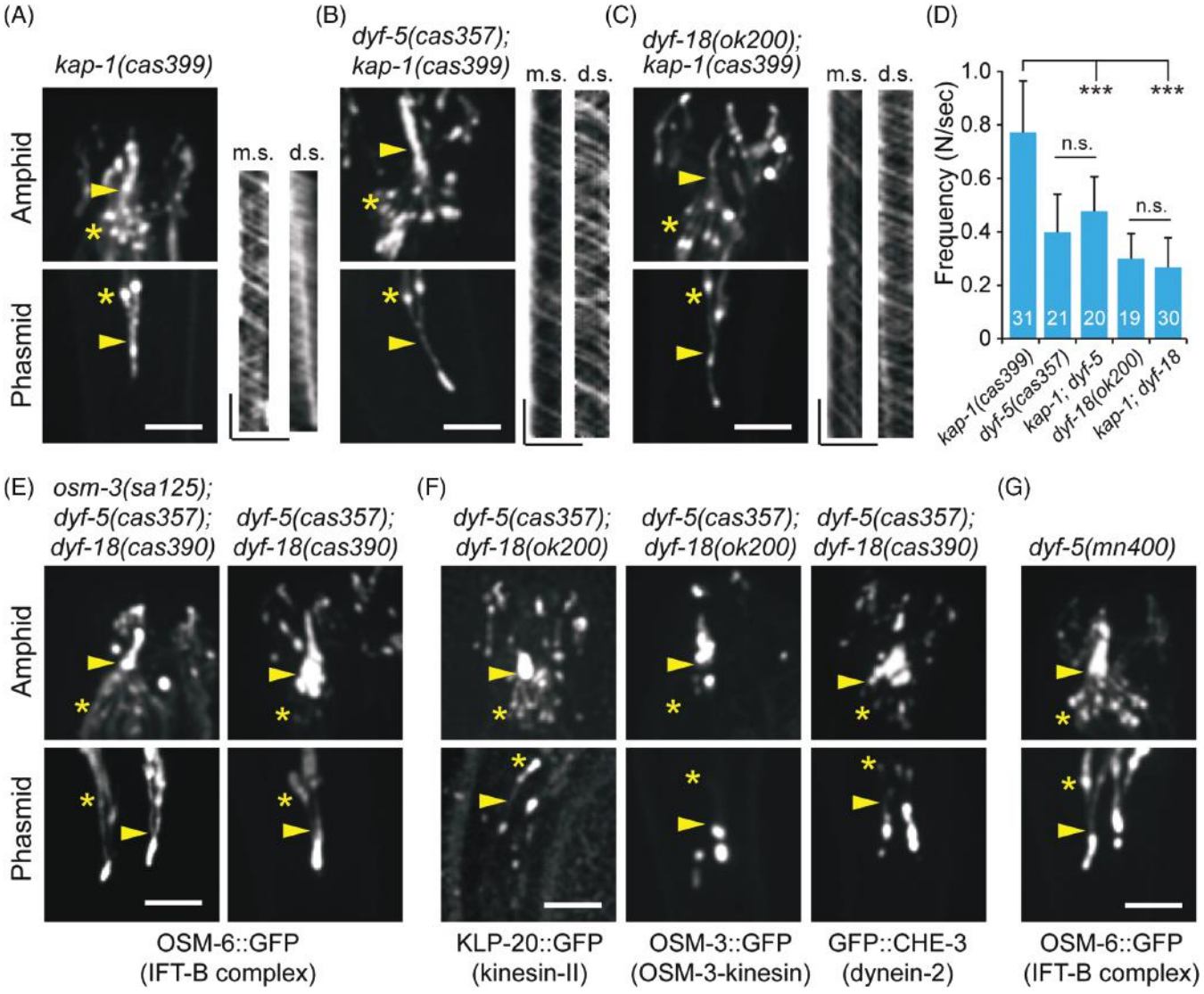

FIGURE 4 *dyf-5* and *dyf-18* regulate the co-ordination between kinesin-II and OSM-3 and the recycling of IFT components. (A) Ciliary phenotypes in the *kap-1* mutant. Cilia are marked with GFP-tagged IFT52/OSM-6. Kymographs show IFT in the middle segment (m.s.) and distal (d.s.) segment. Star, ciliary base; arrowhead, junction between the middle and distal segments; scale in image, 5 μm; scales in kymographs: horizontal, 5 μm; vertical, 5 sec (the same as in [B,C]). (B) Ciliary phenotypes in *dyf-5; kap-1* double mutant. (C) Ciliary phenotypes in *dyf-18; kap-1* double mutant. (D) Quantification of IFT frequencies (mean ±SD.). The numbers of movies used for quantification are shown in the bars. ***, $P < .001$, 2-tailed Student's *t* test. (E) Ciliary phenotypes in the *osm-3; dyf-5; dyf-18* triple mutant and the *dyf-5; dyf-18* double mutant. Star, ciliary base; arrowhead, junction between the middle and distal segments; scale bar, 5 μm (the same as in [F,G]). (F) Ciliary localization of motor proteins in the *dyf-5; dyf-18* double mutants. (G) Ciliary phenotypes in the *dyf-5* null mutant

normal retrograde speeds in these mutants suggest that the recycling defect is probably an indirect result of the failure of handover and IFT-particle reorganization caused by the loss of *dyf-5* and *dyf-18* function. Considering the similar phenotypes observed in *dyf-5* null mutant and *dyf-5(cas357); dyf-18* double mutants (Figure 4G), we speculate that the enhanced phenotypes in the double mutants may not represent the inactivation of parallel pathways but instead may result from exacerbated loss of function of DYF-5 (see Section 3).

2.6 | DYF-5 and DYF-18 are IFT cargo molecules

To determine how DYF-5 and DYF-18 function in cilia, we examined their ciliary localization patterns. We constructed a transgenic animal expressing GFP-tagged DYF-18 that fully rescued the suppression phenotypes in the *osm-3(sa125); dyf-18(cas390)* mutant (Figure 5A,B). DYF-18::GFP localizes to both amphid and phasmid cilia with enrichment at the distal segments and is not detectable at the ciliary base (Figure 5A,D). As overexpression of *dyf-5* causes strong ciliary defects,[26] we generated GFP knock-in at the carboxyl terminus of endogenous isoform a (DYF-5a). The endogenous expression level of DYF-5a is weak in cilia but we detected an enrichment of DYF-5a::GFP fluorescence in the distal segments and ciliary tips (Figure 5C,D). To exclude the effects of kinase activity on cilium formation, we generated transgenic animals expressing GFP-tagged kinase-dead DYF-5 (K40A) or DYF-18(K37A). Both proteins are localized in cilia and show enrichment at the distal segments, but this occurs to a lesser extent compared to the WT proteins (Figure 5E,F). Importantly, our kymograph analyses revealed bidirectional IFT of each protein, indicating

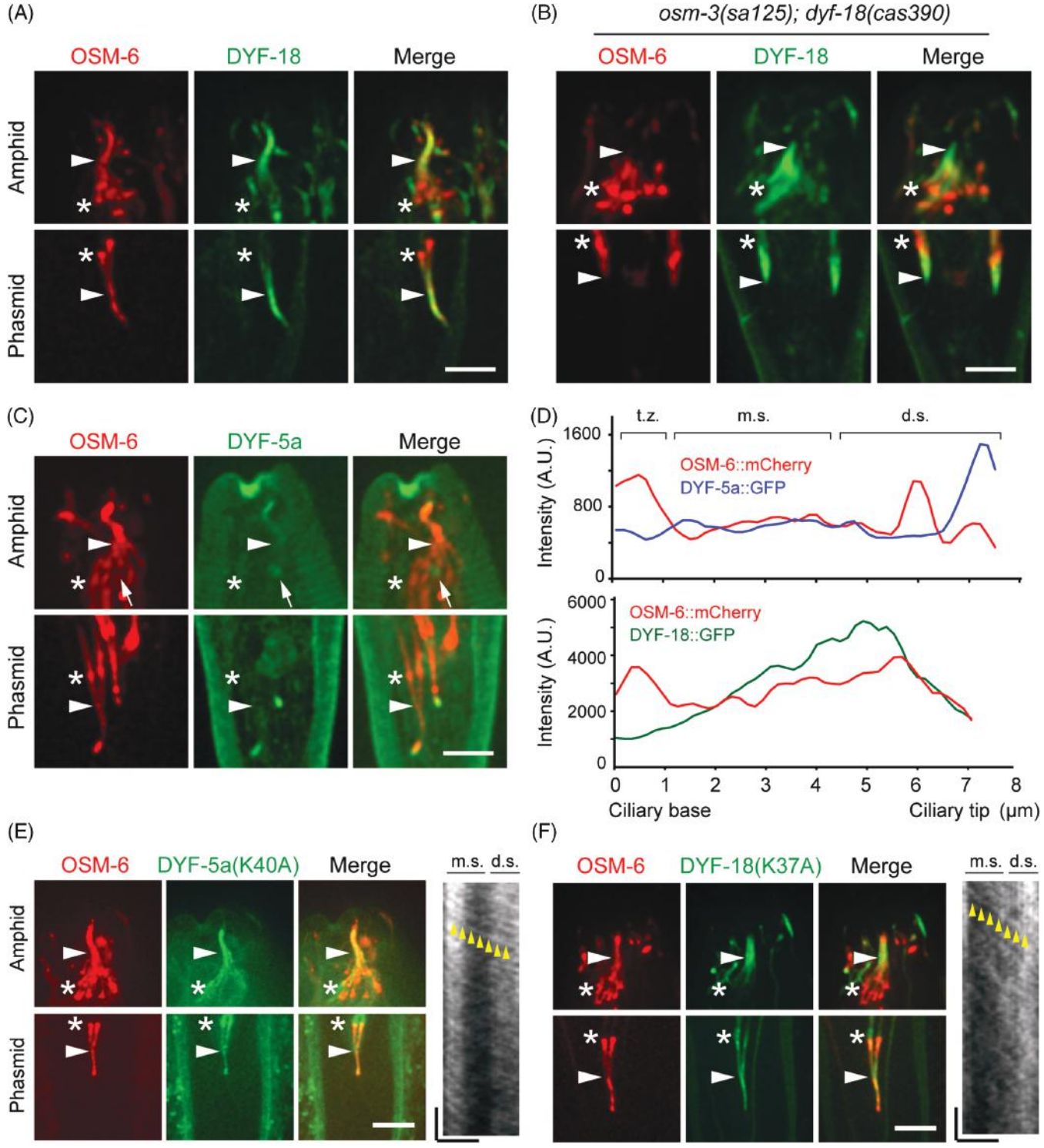

FIGURE 5 DYF-5 and DYF-18 localize to cilia and undergo IFT. (A) Localization of DYF-18 in cilia. DYF-18::GFP and OSM-6::mCherry are expressed under the control of the P*dyf-1* promoter. Star, ciliary base; arrowhead, junction between the middle and distal segments; scale bar, 5 μm (the same as in [B,C]). (B) Expression of DYF-18::GFP rescues the *dyf-18*-dependent suppression of *osm-3(sa125)*. OSM-6::mCherry marks cilia. (C) Endogenous localization of DYF-5a::GFP in cilia. GFP was tagged to the C-terminal end of DYF-5 isoform a by CRISPR/Cas9-mediated knock-in. Arrows indicate autofluorescence. (D) Representative fluorescence intensity of DYF-5a::GFP and DYF-18::GFP along cilia. t.z., transition zone; m.s., middle segment; d.s., distal segment. A.U., arbitrary unit. (E) Ciliary localization and IFT of DYF-5a::GFP bearing the kinase-dead mutation (K40A). DYF-5a(K40A)::GFP and OSM-6::mCherry are expressed under the control of the P*dyf-1* promoter. Star, ciliary base; white arrowhead, junction between the middle and distal segments; yellow arrowheads indicate the movement of a single IFT particle; scale in image, 5 μm; scales in kymographs: horizontal, 5 μm; vertical, 5 seconds. m.s., middle segment; d.s., distal segment (the same as in Figure 5F). (F) Ciliary localization and IFT of DYF-18::GFP bearing the kinase-dead mutation (K37A). DYF-18(K37A)::GFP and OSM-6::mCherry are expressed under the control of the P*dyf-1* promoter

that they are cargo molecules. The velocities of DYF-5 at the middle and distal segments are 0.75 ±0.19 μm/s (mean ±SD, *N* = 77) and 1.25 ±0.22 μm/s (mean ±SD, *N* = 64). DYF-18 moves at speeds of 0.83 ±0.14 μm/s (mean ±SD, *N* = 88) and 1.33 ±0.14 μm/s (mean ±SD, *N* = 40) in the middle and distal segments, respectively. Previous studies report that DYF-5 and DYF-18 localize to the ciliary base.[26,34] The difference in localization patterns may result from overexpression or different experimental conditions. The use of genome-editing techniques and our phenotypic data support that DYF-5 and DYF-18 function at the distal segments or ciliary tips.

2.7 | Kinase activity and ciliary localization are required for DYF-18 function

The isolation of multiple mutations affecting conserved residues in the kinase domains of DYF-5 and DYF-18 underlines the importance of kinase activity in their ciliary functions. To test this possibility, we used the kinase-dead constructs DYF-5(K40A) and DYF-18(K37A) to rescue *osm-3; dyf-5* or *osm-3; dyf-18* mutants, respectively. As expected, both constructs failed to rescue the ciliary phenotypes (Figure 6A,B). Considering that DYF-18 is excluded from the ciliary base (Figure 5A), we asked whether accurate ciliary localization is important for DYF-18 function. To this end, we fused DYF-18 to the transition zone protein MKSR-2. This chimeric protein is localized at the ciliary base and shows weak signal in the putative transition zone (Figure 6C). We found that the phasmid cilia of 11 out of 14 worms became shorter and that the remaining distal segments were not tightly bundled (Figure 6C). These phenotypes were never observed in the cilia of WT or DYF-18 overexpression lines. Our data indicate that proper ciliary localization of DYF-18 is required for its function in ciliogenesis.

3 | DISCUSSION

This study shows that DYF-5 and DYF-18, the *C. elegans* homologs of the mammalian kinases RCK (MAK/ICK/MOK) and CCRK, are IFT cargo molecules that are enriched at the distal segments of sensory cilia. DYF-5 and DYF-18 play critical roles in co-ordinating kinesin-II and OSM-3-kinesin during ciliogenesis and are required for efficient recycling of IFT components (Figure 6D).

3.1 | The interplay between DYF-5 and DYF-18

DYF-5 belongs to the MAP kinase superfamily, members of which contain a canonical TxY motif in the activation loop. Activation of MAP kinases requires autophosphorylation of the tyrosine residue in the TxY motif and subsequent phosphorylation of the threonine residue by other activating kinases.[38] DYF-18 is most closely related to mammalian CCRK and CDK7 which are believed to be cyclin-dependent kinases (CDK)-activating kinases that activate CDK by phosphorylating threonines in their activation loops.[39] However, CDK7, but not CCRK, shows activity toward CDK2.[39] Interestingly, CCRK can phosphorylate and activate ICK and MAK.[31,32] The inhibition of glioblastoma cell proliferation by CCRK depletion is also found to depend on the ciliary functions of ICK and MAK.[23] In addition, genetic analyses in *Chlamydomonas* suggest that *lf2/dyf-18/ccrk* is epistatic to *lf4/dyf-5/ick/mak* during flagellar regeneration.[29] Evidences in our study also suggest DYF-5 and DYF-18 may function in the same pathway: (1) *dyf-5* mutants with hypomorphic alleles and the *dyf-18* null mutant show similar phenotypes; (2) their double mutants form aggregates, similar to *dyf-5* null mutant (Figure 4E,G) and (3) DYF-5 and DYF-18 show similar localization patterns. In mammalian cells, autophosphorylation of Y159 in the ICK TxY motif confers basal kinase activity, and ICK is fully activated by additional phosphorylation of T157.[40] It is probably that the ciliary functions of DYF-5 require autophosphorylation and activation by DYF-18. Loss of *dyf-18* reduces but does not abolish DYF-5 activity, which mimics partial loss of function caused by *dyf-5* weak alleles. The enhanced ciliary defects in *dyf-18*; *dyf-5(weak allele)* double mutants may result from the additive effects on the loss of DYF-5 activity, which is evidenced by almost identical phenotypes in *dyf-18*; *dyf-5(weak allele)* double-mutant and *dyf-5*-null animals (Figure 4E,G). Our imaging data further show that DYF-5 and DYF-18 exhibit similar localization patterns, supporting the possibility of their interaction in vivo (Figure 5). However, the ciliary localization of DYF-5 does not depend on DYF-18, suggesting that the regulation of DYF-5 localization and DYF-5 activity can be separated (Figure S3 in Appendix S1).

Overexpression of *dyf-5* or its homologs in *Leishmania mexicana* and mammalian cells causes shorter cilia, indicating that a negative regulatory mechanism is also essential for *dyf-5* function.[20,22,26,27] Similar phenotypes are observed when CCRK is overexpressed.[23] In cancer cells, overexpression of MAK and CCRK also inhibits ciliogenesis, leading to increased cell proliferation.[32,41] Phylogenetically, MAK and CCRK are related to cell cycle-associated kinases, which implies that they might participate in a CDK-like signaling pathway. Interestingly, the threonine in the activation loop of CCRK is replaced with an aspartic acid in DYF-18 (Figure S1B in Appendix S1), which explains why overexpression of DYF-18 does not affect ciliogenesis in *C. elegans*. In addition to CCRK, ICK and MAK, other cell cycle-associated kinases, such as never in mitosis gene a (NIMA)-related kinases and CDK-like kinases, are also found to regulate cilium length.[42–46] We speculate that a complex signaling cascade involving multiple cell cycle-associated kinases may function to inhibit ciliogenesis, although the relationship between these kinases remains to be addressed in the future. Importantly, our suppressor screen also identifies an NIMA kinase-like gene, *nekl-4*, which encodes the mammalian NEK10 homolog as a suppressor of *osm-3(sa125)* (Figure S4 in Appendix S1). NEKL-4 localizes to the ciliary compartment, and its loss of function only shows mild suppression phenotypes.

3.2 | DYF-5 and DYF-18 regulate the motility of kinesin-II and OSM-3-kinesin

We show that DYF-5 and DYF-18 may regulate the handover of IFT particles between kinesin-II and OSM-3 (Figure 6D). In the *osm-3 (sa125)* mutant, distal segments cannot be assembled due to the normal handover and the defects of OSM-3 motility. Without *dyf-5* or *dyf-18* kinase activity, the handover becomes defective, which leads to the prolonged activation and ectopic entry of kinesin-II. This model

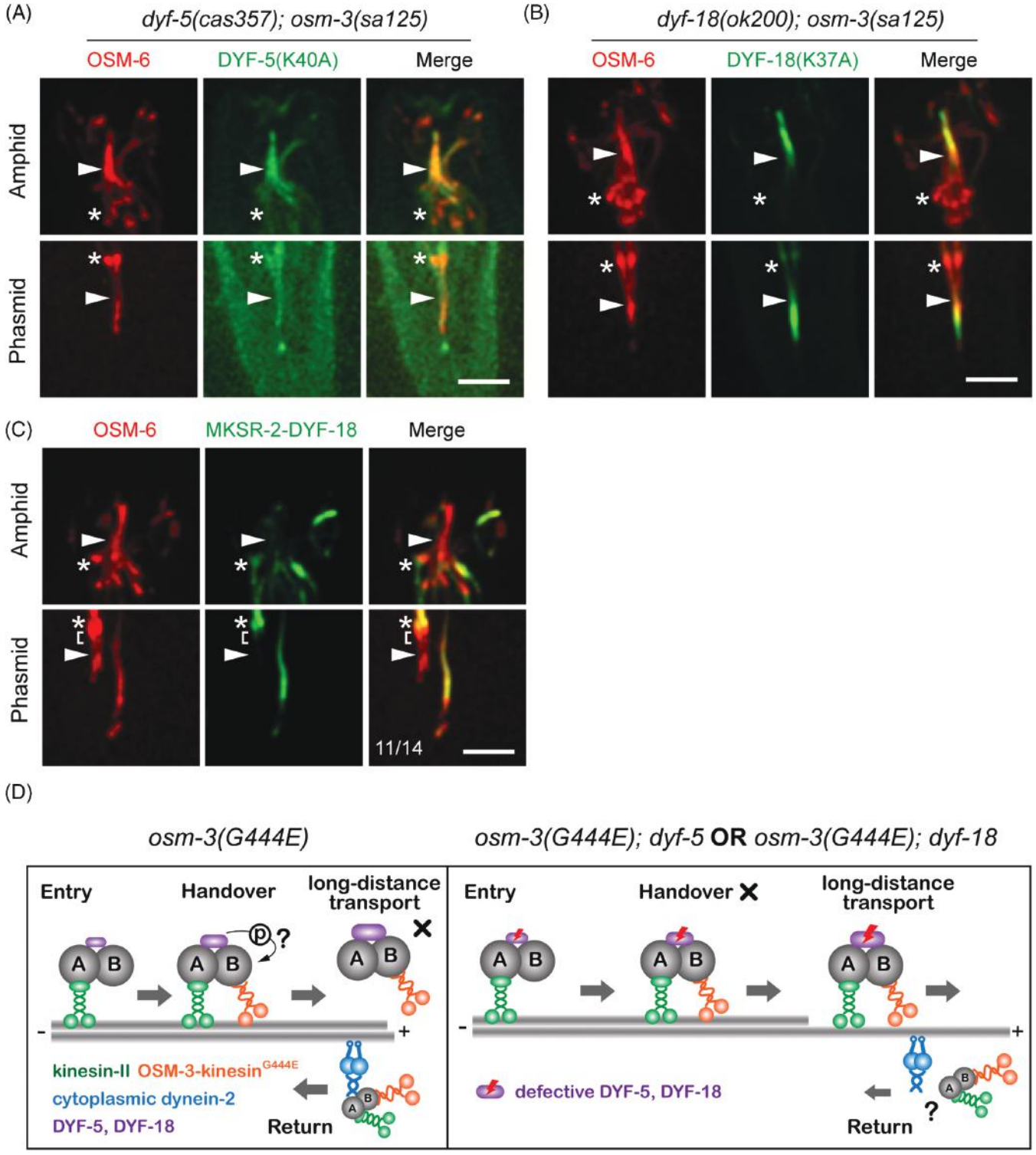

FIGURE 6 Requirement of kinase activity and localization for DYF-5 and DYF-18 function and a proposed model. (A-B) Kinase-dead DYF-5 (K40A) or DYF-18(K37A) does not rescue the suppression of *osm-3(sa125).* DYF-5a(K40A)::GFP, DYF-18(K37A)::GFP and OSM-6::mCherry are expressed under the control of the P*dyf-1* promoter. Star, ciliary base; arrowhead, junction between the middle and distal segments; scale bar, 5 μm (the same as in [C]). (C) Ectopic localization of DYF-18 causes alignment defects in phasmid cilia (11 out of 14 animals). Note that the distal segments are not well-bundled. DYF-18 is fused with transition zone protein MKSR-2 and GFP. This chimeric protein is mainly localized to the ciliary base and putative transition zone region (indicated by brackets). (D) A model illustrating the regulation of kinesin-II and OSM-3 by DYF-5 and DYF-18. DYF-5 and DYF-18 are transported into cilia as cargo molecules. With the increases in protein level and probably kinase activity at the tip of middle segment, DYF-5 and DYF-18 are sufficient to trigger the handover of IFT particles between kinesin-II and OSM-3, possibly through phosphorylation of IFT components. In the *osm-3(G444E)* mutant, the handover is normal. However, as OSM-3(G444E) motility is severely compromised, the long-distance transport and assembly of the distal segment are blocked. In *osm-3(G444E); dyf-15* or *osm-3(G444E); dyf-18* mutants, the handover is defective, resulting in the failure of kinesin-II undocking and inactivation. Distal segment assembly is partially restored by kinesin-II-triggered long-distance transport; however, inaccurately organized IFT particles may indirectly affect the efficiency of recycling

is consistent with a previous report that DYF-5 is required for kinesin-II undocking and OSM-3 docking.[26] Interestingly, *dyf-5* mutation also suppresses the Dyf phenotype of *osm-3(null)*, but the efficiency is much lower than that in *dyf-5; osm-3(sa125)* double-mutant animals, which suggests that OSM-3 may also play a structural role in maintaining IFT particles in a state favorable for kinesin-II transport. This finding is consistent with a previous report that IFT particles driven by kinesin-II alone are less well-organized.[13] In addition, DYF-5 and DYF-18 also participate in regulating IFT-particle recycling. Although the recycling defects in their mutants may be explained by the increased IFT import and imbalanced bidirectional IFT due to the failure of kinesin-II undocking, we propose that these defects are indirect consequences, given that OSM-3-driven anterograde IFT is also impaired in the absence of *dyf-5*,[26] and importantly, that retrograde speeds in our mutants are generally normal. We propose that the handover is tightly coupled with IFT-particle reorganization. Failure of handover impairs proper IFT-particle reorganization, which is required for retrograde transport initiation at the ciliary tips.[37] In addition, we observed ciliary transport of DYF-5 and DYF-18 and enriched localization at distal segments or ciliary tips (Figure 5). Together with the requirement of an appropriate amount of DYF-5,[26] our results suggest a cargo-dependent feedback mechanism that controls kinesin-II activity and cilium length. Interestingly, the phosphorylation and activation status of an Aurora-like kinase also correlate with flagellar length in *Chlamydomonas*.[47,48]

How does DYF-5 regulate kinesin-II localization? It is possible that DYF-5 inhibits kinesin-II activity via direct phosphorylation. To test this possibility, we performed GFP-based affinity purification of kinesin-II and mass spectrometry to identify phosphorylation sites. We identified 2 phosphorylated residues, Ser102 on KAP-1/KAP and Ser735 on KLP-11/KIF3B (Figure S5 in Appendix S1). However, neither the Ser-to-Ala nor Ser-to-Asp mutations could localize kinesin-II to the distal segments. In addition, phosphorylation does not disappear in the absence of *dyf-5*. These data suggest that phosphorylation of kinesin-II is not essential for its localization or that phosphorylation on other residues is undetectable under our conditions. Alternatively, DYF-5 may indirectly regulate kinesin-II activity by acting on other IFT components. In *zebra fish* photoreceptors, the IFT-B component IFT57 is required for the ATP-dependent dissociation of kinesin-II from IFT particles.[49] *Chlamydomonas* kinesin-II can be phosphorylated and inactivated by the CDPK1 kinase,[19] but to our knowledge, no direct interactions between the DYF-5 homolog LF4 and kinesin-II have been reported.

Our GFP affinity purification and mass spectrometry analyses did not uncover any phosphorylation on OSM-3, raising the possibility that DYF-5 may act on IFT particles to regulate kinesin-II and OSM-3 indirectly. The *C. elegans* BBSome components could be potential candidates because loss of *bbs-7* or *bbs-8* separates IFT-A and IFT-B subcomplexes, and importantly, the BBSome modulates the competition between kinesin-II and OSM-3.[12,50] The BBSome also interacts with IFT-A components to regulate the turnaround of IFT particles.[37] Other potential candidates include OSM-3 activators, such as DYF-13, DYF-1, DYF-6, IFT-74 and IFT-81, among which IFT-74/IFT81 can bind to OSM-3.[51] The handover between kinesin-II and OSM-3 may be coupled with the inactivation of kinesin-II and activation of OSM-3 through cargo undocking and docking.[26] As *C. elegans* kinesin-II only moves on the middle segment, which is composed of doublet microtubules,[8] the bipartite axonemal structure might also be involved in regulating kinesin-II. However, that is unlikely because the *dyf-5* mutant contains singlet microtubules in the distal segments.[26]

4 | MATERIALS AND METHODS

4.1 | Strain culture and genetics

All strains were raised on the nematode growth medium (NGM) plates seeded with *Escherichia coli* OP50 at 20°C. The genotypes of strains used in this study were listed in Table S1 in Appendix S1. To isolate *osm-3(sa125)* suppressors, *mnIs17[OSM-6::GFP]; osm-3(sa125)* mutant animals (P0) were synchronized at the late L4 stage, collected in 4 mL M9 buffer, and incubated with 50 mM ethyl methanesulfonate (EMS) for 4 hours at room temperature with constant rotation. Animals were then washed with M9 for 3 times and cultured under standard conditions. 30 hours later, gravid animals were bleached. Eggs (F1) were distributed and raised on ~100 9-cm-NGM plates, each containing 50 to 100 eggs. Adult F2 animals on each plate were collected and subjected to dye filling (see Dye-filling assay). Dye-positive mutant animals were individually cultured and their progenies were double-checked via the dye-filling assay and the microscopic examination of ciliary phenotypes. To map the mutations, a putative null allele *cas370* of *osm-3* (8 bp deletion at exon 2) was introduced into the CB4856 strain by CRISPR/Cas9 knockout. Suppressor mutants were crossed with this strain to perform single-nucleotide polymorphism mapping. Mutations were identified by whole genome sequencing. Isolated mutants were outcrossed for 3 times. Adult hermaphrodite worms were used in the dye-filling assays and the live imaging experiments. Worms at mixed stages were collected to perform GFP immunoprecipitation and mass spectrometry. All animal experiments were performed in accordance with the governmental and institutional guidelines.

4.2 | Molecular biology

The OSM-3(ΔH2) cDNA was a gift from Ronald Vale lab. OSM-3 (G444E) coding sequence was amplified from the *osm-3(sa125)* mutant genomic DNA. Constructs for overexpression of OSM-3 (ΔH2), OSM-3(G444E), OSM-6, DYF-5a(K40A), DYF-18(K37A), TBB-4, NEKL-4 and kinesin-II subunits were generated by inserting their coding sequences into the pDONR vectors that contain the ~400 bp *dyf-1* promoter and GFP/mCherry::*unc-54* 3′UTR using In-Fusion Advantage polymerase chain reaction (PCR) cloning kit (Clontech, cat. no. 639621). For OSM-3(G444E), OSM-6, DYF-5a(K40A), DYF-18 (K37A) and TBB-4, genomic sequences were used. For OSM-3(ΔH2), NEKL-4, KAP-1a and KLP-11a, cDNA sequences were used. Point mutations were introduced by transforming linearized the vectors with 15 bp overlapping ends, which bear necessary mutations, into DH5α bacteria after WT sequences were cloned into the pDONR vectors. DYF-18::GFP or TBA-5::GFP fusion constructs were generated by SOEing PCR of the genomic sequences that contain their

promoters and coding regions with the GFP::*unc-54* 3'UTR fragment, respectively. Approximately 900 bp promoter of *dyf-18* and ~5 kb promoter of *tba-5* were used, respectively. MKSR-2::DYF-18::GFP expression vector was obtained by inserting the MKSR-2 genomic coding sequence into the P*dyf-1*::*dyf-18*::*GFP* plasmid. For heat-shock inducible expression, the *dyf-1* promoter was replaced with the ~400 bp *hsp-16.2* promoter. Primers used in this study were listed in Table S2 in Appendix S1.

4.3 | Knockout and knock-in

CRISPR targets were inserted to the pDD162 vector (Addgene #47549) in the same way as introducing point mutations. Target sequences for *dyf-18*, *kap-1* and *osm-3* knockout were AGGAAGTACCGTATACGTT (AGG), ATGCACACCCGTCAGATC (AGG) and ATGGCACTGTGTTTGCCTA (TGG) in which the protospacer adjacent motifs were shown in the brackets. Two targets GAAGAAAGGCATGCGCCAAA (AGG) and CAATTGCAAACACTAAGAATAT (AGG) were used to generate DYF-5a::GFP knock-in strain. The homology arms are 850 bp (5′) and 1200 bp (3′) in length, and were cloned into the pPD95.77 vector. GFP sequence was inserted prior to the stop codon. The last 11 amino acids of DYF-5a were removed to prevent the homology templates from Cas9 cutting. CRISPR/Cas9 constructs at a concentration of ~50 ng/μL were microinjected into the germ line of young adult hermaphrodites (*mnIs17[OSM-6::GFP]; osm-3(sa125)* mutant strain for *dyf-18* and *kap-1* knockout, CB4856 for *osm-3* knockout and WT N2 for *dyf-5* knock-in) together with *rol-6[su1006]* and P*odr-1*::*dsRed* markers. Roller and red fluorescence positive F1s were individually cultured. Successful edited animals were screened by PCR amplification and sequencing of mixed F2 progenies. Homozygous F2 animals without extrachromosomal transgenic markers were screened and verified by sequencing. The *osm-3* mutant allele, *cas370* in CB4856, is an 8-bp deletion "GTTTGCCT" at exon 2. The *kap-1* allele *cas399* is a 14-bp deletion "CGTCAGATCAGGCA" at exon 1. The *dyf-18* allele *cas444* is a compound mutation that bears a 3-bp deletion and a 58-bp insertion "TACCGTATA/TAGGGGATATTATTAAAGACAAAACACGACCTGATGTCAATTGTTACCGAGGAAGTACCGTTAG" (flanking sequences are underlined) at exon 3. All 3 mutations introduce frame shifts and premature stop codons, thus are putative null alleles.

4.4 | Transgenesis

Transgenic lines of OSM-3(G444E)::GFP, OSM-3(ΔH2)::GFP, TBA-5::GFP, TBB-4:mCherry, DYF-18::GFP, DYF-5(K40A)::GFP, DYF-18(K37A)::GFP, MKSR-2::DYF-18::GFP, NEKL-4::GFP and kinesin-II::GFP/mCherry were obtained by injecting these constructs with appropriate selection markers (*rol-6(su1006)* or P*dyf-1*::*osm-6*::*mCherry*) into the germ line of WT N2 or mutant young adult animals. Marker-positive F1s were individually cultured. Transgenic lines were maintained if F2s inherited the transgenes. Concentration of each DNA construct for microinjection was ~50 ng/μL. Similar expression patterns were observed in at least 2 independent lines of each transgenic strain.

4.5 | Dye-filling assay

Adult animals were collected into ~200 μL M9 buffer, washed for 2 times, and mixed with equal volume of fluorescence dye (DiI 1,1′-dioctadecyl-3,3,3′,3′,-tetramethylindocarbocyanine perchlorate, Sigma) at a concentration of 20 μg/mL. After incubation at room temperature in dark for 30 to 60 minutes, animals were transferred to seeded NGM plates and allowed to excrete excess intestinal dye. One hour later, animals were examined for dye filling in the head and tail sensory neurons via microscopy.

4.6 | Live imaging and analysis

Adult animals were immobilized with 0.1 mmol/L levamisole in M9 buffer on 3% agar pads in round-bottom dishes and maintained at room temperature for imaging of ciliary morphology and IFT. Our imaging system includes an Axio Observer Z1 microscope (Carl Zeiss) equipped with a ×100, 1.46 numerical aperture objective lens, an EMCCD camera (iXon+ DU-897D-C00-#BV-500; Andor Technology), and the 405, 488 and 568 nm lines of a Sapphire CW CDRH USB Laser System (Coherent) with a spinning disk confocal scan head (CSU-X1 Spinning Disk Unit; Yokogawa Electric Corporation). Images were acquired by μManager (www.micro-manager.org). Still images were taken at an exposure time of 100 to 200 milliseconds, and time-lapse images showing IFT were acquired at an exposure time of 200 milliseconds. Laser power was 20% to 30%. Kymograph extraction, image processing and measurement of cilium length and IFT speeds were performed in ImageJ (http://rsbweb.nih.gov/ij/). Amphid and phasmid cilia were randomly selected for cilium-length and IFT quantification. For cilium-length measurement, individual phasmid cilium was measured, but in each amphid sensillum, average length of multiple cilia was used as a single value for quantification. Because the ciliary distal segments form bundles, IFT frequency was only quantified in the middle segments, where an individual cilium can be faithfully determined.

4.7 | Bioinformatics

Sequence alignment was performed using Clustal X2.1 (http://www.clustal.org/). Protein sequences were obtained from Wormbase (http://www.wormbase.org/) or National Center for Biotechnology Information (www.ncbi.nlm.nih.gov/). Conserved domains were identified by SMART (simple modular architecture research tool) (http://smart.embl-heidelberg.de/) or CDD (NCBI's conserved domain database) online tools. Sequence IDs used include CAQ76489.2 (*Ce*DYF-5), P20794.2 (*Hs*MAK), NP_055735.1 (*Hs*ICK), BAA81688.1 (*Hs*MOK), AAO86687.1 (*Cr*LF4), CAA43985.1 (*Hs*CDK2), CAB07422.2 (*Ce*DYF-18), NP_001034892.1 (*Hs*CCRK), ABK34486.1 (*Cr*LF2), NP_001790.1 (*Hs*CDK7), NP_001186326.1 (*Hs*NEK1), NP_002488.1 (*Hs*NEK2), NP_002489.1 (*Hs*NEK3), NP_003148.2 (*Hs*NEK4), NP_954983.1 (*Hs*NEK5), CAG33372.1 (*Hs*NEK6), BAB85632.1 (*Hs*NEK7), AAP04006.1 (*Hs*NEK8), NP_149107.4 (*Hs*NEK9), NP_689747.3 (*Hs*NEK10), NP_079076.3 (*Hs*NEK11), NP_001293320.1 (*Ce*NEKL-1), NP_491914.1 (*Ce*NEKL-2), NP_510080.2 (*Ce*NEKL-3) and NP_498178.3 (*Ce*NEKL4). Full sequences were used to perform alignment except *Hs*NEK10 and *Ce*NEKL-4 whose kinase domains were used.

4.8 | Quantification and statistical analysis

Quantification was represented by the mean value ±SD for each group. Two-tailed Student's *t* test analysis was performed to examine all significant differences between groups as indicated in the figure legends. The numbers of subjects (animals, cilia or movies) used for quantification were indicated in the figure legends. Significance was determined when the *P* value is <.05. The variance is not significantly different between groups that are being compared unless it is mentioned in the text.

ACKNOWLEDGMENTS

We thank Caenorhabditis Genetics Center (CGC) for providing some strains. We thank the Protein Chemistry Facility at the Center for Biomedical Analysis of Tsinghua University for mass spectrometry and sample analysis. This work was supported by the National Basic Research Program of China (grant 2017YFA0503501), the National Natural Science Foundation of China (grants 31525015 and 31561130153) and the Newton Advanced Fellowship from the Royal Society (grant 140490).

Author contributions

G.O. and P.Y. conceived this project. P.Y. and C.X. performed the experiments. P.Y. collected and analyzed the data under the supervision of G.O. G.O. and P.Y. wrote the manuscript.

Conflict of interest

The authors declare no competing financial interests.

Editorial Process File: The Editorial Process File is available in the online version of this article.

ORCID

Peishan Yi http://orcid.org/0000-0003-4710-8089

REFERENCES

1. Ishikawa H, Marshall WF. Intraflagellar transport and ciliary dynamics. *Cold Spring Harb Perspect Biol*. 2017;9(3): pii: a021998.
2. Rosenbaum JL, Witman GB. Intraflagellar transport. *Nat Rev Mol Cell Biol*. 2002;3(11):813-825.
3. Scholey JM. Intraflagellar transport. *Annu Rev Cell Dev Biol*. 2003;19:423-443.
4. Taschner M, Lorentzen E. The intraflagellar transport machinery. *Cold Spring Harb Perspect Biol*. 2016;8(10):a028092.
5. Ishikawa H, Marshall WF. Ciliogenesis: building the cell's antenna. *Nat Rev Mol Cell Biol*. 2011;12(4):222-234.
6. Kozminski KG, Johnson KA, Forscher P, Rosenbaum JL. A motility in the eukaryotic flagellum unrelated to flagellar beating. *Proc Natl Acad Sci USA*. 1993;90(12):5519-5523.
7. Scholey JM. Kinesin-2: a family of heterotrimeric and homodimeric motors with diverse intracellular transport functions. *Annu Rev Cell Dev Biol*. 2013;29:443-469.
8. Snow JJ, Ou G, Gunnarson AL, et al. Two anterograde intraflagellar transport motors cooperate to build sensory cilia on *C. elegans* neurons. *Nat Cell Biol*. 2004;6(11):1109-1113.
9. Signor D, Wedaman KP, Rose LS, Scholey JM. Two heteromeric kinesin complexes in chemosensory neurons and sensory cilia of Caenorhabditis elegans. *Mol Biol Cell*. 1999;10(2):345-360.
10. Evans JE, Snow JJ, Gunnarson AL, et al. Functional modulation of IFT kinesins extends the sensory repertoire of ciliated neurons in Caenorhabditis elegans. *J Cell Biol*. 2006;172(5):663-669.
11. Inglis PN, Ou G, Leroux MR, Scholey JM. The sensory cilia of Caenorhabditis elegans. *WormBook*. 2007;1-22.
12. Ou G, Blacque OE, Snow JJ, Leroux MR, Scholey JM. Functional coordination of intraflagellar transport motors. *Nature*. 2005;436(7050):583-587.
13. Prevo B, Mangeol P, Oswald F, Scholey JM, Peterman EJ. Functional differentiation of cooperating kinesin-2 motors orchestrates cargo import and transport in *C. elegans* cilia. *Nat Cell Biol*. 2015;17(12):1536-1545.
14. Verhey KJ, Hammond JW. Traffic control: regulation of kinesin motors. *Nat Rev Mol Cell Biol*. 2009;10(11):765-777.
15. Hammond JW, Blasius TL, Soppina V, Cai D, Verhey KJ. Autoinhibition of the kinesin-2 motor KIF17 via dual intramolecular mechanisms. *J Cell Biol*. 2010;189(6):1013-1025.
16. Imanishi M, Endres NF, Gennerich A, Vale RD. Autoinhibition regulates the motility of the *C. elegans* intraflagellar transport motor OSM-3. *J Cell Biol*. 2006;174(7):931-937.
17. Wedaman KP, Meyer DW, Rashid DJ, Cole DG, Scholey JM. Sequence and submolecular localization of the 115-kD accessory subunit of the heterotrimeric kinesin-II (KRP85/95) complex. *J Cell Biol*. 1996;132(3):371-380.
18. Brunnbauer M, Mueller-Planitz F, Kosem S, et al. Regulation of a heterodimeric kinesin-2 through an unprocessive motor domain that is turned processive by its partner. *Proc Natl Acad Sci USA*. 2010;107(23):10460-10465.
19. Liang Y, Pang Y, Wu Q, et al. FLA8/KIF3B phosphorylation regulates kinesin-II interaction with IFT-B to control IFT entry and turnaround. *Dev Cell*. 2014;30(5):585-597.
20. Moon H, Song J, Shin JO, et al. Intestinal cell kinase, a protein associated with endocrine-cerebro-osteodysplasia syndrome, is a key regulator of cilia length and Hedgehog signaling. *Proc Natl Acad Sci USA*. 2014;111(23):8541-8546.
21. Chaya T, Omori Y, Kuwahara R, Furukawa T. ICK is essential for cell type-specific ciliogenesis and the regulation of ciliary transport. *EMBO J*. 2014;33(11):1227-1242.
22. Broekhuis JR, Verhey KJ, Jansen G. Regulation of cilium length and intraflagellar transport by the RCK-kinases ICK and MOK in renal epithelial cells. *PloS One*. 2014;9(9):e108470.
23. Yang Y, Roine N, Makela TP. CCRK depletion inhibits glioblastoma cell proliferation in a cilium-dependent manner. *EMBO Rep*. 2013;14(8):741-747.
24. Omori Y, Chaya T, Katoh K, et al. Negative regulation of ciliary length by ciliary male germ cell-associated kinase (Mak) is required for retinal photoreceptor survival. *Proc Natl Acad Sci USA*. 2010;107(52):22671-22676.
25. Tam LW, Wilson NF, Lefebvre PA. A CDK-related kinase regulates the length and assembly of flagella in Chlamydomonas. *J Cell Biol*. 2007;176(6):819-829.
26. Burghoorn J, Dekkers MP, Rademakers S, de Jong T, Willemsen R, Jansen G. Mutation of the MAP kinase DYF-5 affects docking and undocking of kinesin-2 motors and reduces their speed in the cilia of Caenorhabditis elegans. *Proc Natl Acad Sci USA* 2007;104(17):7157–7162.
27. Bengs F, Scholz A, Kuhn D, Wiese M. LmxMPK9, a mitogen-activated protein kinase homologue affects flagellar length in Leishmania mexicana. *Mol Microbiol*. 2005;55(5):1606-1615.
28. Berman SA, Wilson NF, Haas NA, Lefebvre PA. A novel MAP kinase regulates flagellar length in Chlamydomonas. *Curr Biol*. 2003;13(13):1145-1149.
29. Asleson CM, Lefebvre PA. Genetic analysis of flagellar length control in Chlamydomonas reinhardtii: a new long-flagella locus and extragenic suppressor mutations. *Genetics*. 1998;148(2):693-702.
30. Snouffer A, Brown D, Lee H, et al. Cell cycle-related kinase (CCRK) regulates ciliogenesis and Hedgehog signaling in mice. *PLoS Genet*. 2017;13(8):e1006912.
31. Fu Z, Larson KA, Chitta RK, et al. Identification of yin-yang regulators and a phosphorylation consensus for male germ cell-associated kinase (MAK)-related kinase. *Mol Cell Biol*. 2006;26(22):8639-8654.

32. Wang LY, Kung HJ. Male germ cell-associated kinase is overexpressed in prostate cancer cells and causes mitotic defects via deregulation of APC/CCDH1. *Oncogene*. 2012;31(24):2907-2918.
33. Ko HW, Norman RX, Tran J, Fuller KP, Fukuda M, Eggenschwiler JT. Broad-minded links cell cycle-related kinase to cilia assembly and hedgehog signal transduction. *Dev Cell*. 2010;18(2):237-247.
34. Phirke P, Efimenko E, Mohan S, et al. Transcriptional profiling of *C. elegans* DAF-19 uncovers a ciliary base-associated protein and a CDK/CCRK/LF2p-related kinase required for intraflagellar transport. *Dev Biol*. 2011;357(1):235-247.
35. Nachury MV, Loktev AV, Zhang Q, et al. A core complex of BBS proteins cooperates with the GTPase Rab8 to promote ciliary membrane biogenesis. *Cell*. 2007;129(6):1201-1213.
36. Efimenko E, Bubb K, Mak HY, et al. Analysis of xbx genes in *C. elegans*. *Development*. 2005;132(8):1923-1934.
37. Wei Q, Zhang Y, Li Y, Zhang Q, Ling K, Hu J. The BBSome controls IFT assembly and turnaround in cilia. *Nat Cell Biol*. 2012;14(9):950-957.
38. Cobb MH, Goldsmith EJ. How MAP kinases are regulated. *J Biol Chem*. 1995;270(25):14843-14846.
39. Wohlbold L, Larochelle S, Liao JC, et al. The cyclin-dependent kinase (CDK) family member PNQALRE/CCRK supports cell proliferation but has no intrinsic CDK-activating kinase (CAK) activity. *Cell Cycle*. 2006;5(5):546-554.
40. Fu Z, Schroeder MJ, Shabanowitz J, et al. Activation of a nuclear Cdc2-related kinase within a mitogen-activated protein kinase-like TDY motif by autophosphorylation and cyclin-dependent protein kinase-activating kinase. *Mol Cell Biol*. 2005;25(14):6047-6064.
41. Ng SS, Cheung YT, An XM, et al. Cell cycle-related kinase: a novel candidate oncogene in human glioblastoma. *J Natl Cancer Inst*. 2007;99(12):936-948.
42. Hilton LK, Gunawardane K, Kim JW, Schwarz MC, Quarmby LM. The kinases LF4 and CNK2 control ciliary length by feedback regulation of assembly and disassembly rates. *Curr Biol*. 2013;23(22):2208-2214.
43. Tam LW, Ranum PT, Lefebvre PA. CDKL5 regulates flagellar length and localizes to the base of the flagella in Chlamydomonas. *Mol Biol Cell*. 2013;24(5):588-600.
44. Bradley BA, Quarmby LM. A NIMA-related kinase, Cnk2p, regulates both flagellar length and cell size in Chlamydomonas. *J Cell Sci*. 2005;118(Pt 15):3317-3326.
45. Meng D, Pan J. A NIMA-related kinase, CNK4, regulates ciliary stability and length. *Mol Biol Cell*. 2016;27(5):838-847.
46. Canning P, Park K, Goncalves J, et al. CDKL family kinases have evolved distinct structural features and ciliary function. *Cell Rep*. 2018;22(4):885-894.
47. Cao M, Meng D, Wang L, Bei S, Snell WJ, Pan J. Activation loop phosphorylation of a protein kinase is a molecular marker of organelle size that dynamically reports flagellar length. *Proc Natl Acad Sci USA*. 2013;110(30):12337-12342.
48. Luo M, Cao M, Kan Y, Li G, Snell W, Pan J. The phosphorylation state of an aurora-like kinase marks the length of growing flagella in Chlamydomonas. *Curr Biol*. 2011;21(7):586-591.
49. Krock BL, Perkins BD. The intraflagellar transport protein IFT57 is required for cilia maintenance and regulates IFT-particle-kinesin-II dissociation in vertebrate photoreceptors. *J Cell Sci*. 2008;121(11):1907-1915.
50. Pan X, Ou G, Civelekoglu-Scholey G, et al. Mechanism of transport of IFT particles in C. Elegans cilia by the concerted action of kinesin-II and OSM-3 motors. *J Cell Biol*. 2006;174(7):1035-1045.
51. Hao L, Thein M, Brust-Mascher I, et al. Intraflagellar transport delivers tubulin isotypes to sensory cilium middle and distal segments. *Nat Cell Biol*. 2011;13(7):790-798.

SUPPORTING INFORMATION

Additional supporting information may be found online in the Supporting Information section at the end of the article.

How to cite this article: Yi P, Xie C, Ou G. The kinases male germ cell-associated kinase and cell cycle-related kinase regulate kinesin-2 motility in *Caenorhabditis elegans* neuronal cilia. *Traffic*. 2018;19:522–535. https://doi.org/10.1111/tra.12572